Hindawi
International Journal of Aerospace Engineering
Volume 2022, Article ID 7169123, 16 pages
https://doi.org/10.1155/2022/7169123

Research Article

Parametric Influences of Geometric Dimensions on High Temperature Mechanical Behaviors and Damage Mechanisms of Ceramic Matrix Composite and Superalloy Double Bolted Joints

Shuyuan Zhao,[1] **Qian Sun**,[2] **Yumin Zhang**,[1] **and Jin Jia**[3]

[1]*National key Laboratory of Science and Technology on Advanced Composites in Special Environments, Harbin Institute of Technology, Harbin 150080, China*
[2]*Shenyang Aircraft Design and Research Institute, Aviation Industry Corporation of China, Shenyang 110000, China*
[3]*School of Materials Science and Engineering, Harbin Institute of Technology, Harbin 150001, China*

Correspondence should be addressed to Shuyuan Zhao; angel.zsy@126.com and Qian Sun; sunqian601@163.com

Received 30 May 2022; Accepted 29 July 2022; Published 31 August 2022

Academic Editor: Xianfeng Yang

Given multiple material performance advantages, ceramic matrix composite (CMC) material has become one of the most promising hot structural materials used for thermal protection system in hypersonic vehicles. Under harsh thermal exposure of vehicles in flight, the design of connection structure would be a critical issue in improving load-carrying efficiency and ensuring service safety of aircraft structures in service environments. However, little attention was paid on mechanical behavior and its factors affecting the mechanical property of CMC joining at elevated temperature. To address this concern, a 3D finite element model coupled with progressive damage analysis is carried out to predict high temperature tensile properties and failure behavior of single-lap, double-bolt CMC/superalloy joints assembled by two serial protruding-head bolts. In the implementation of progressive damage analysis of 2D plain-woven C/SiC composites, a user-defined subroutine UMAT including a nonlinear constitutive model, 3D Alvaro failure criterion and Tan's material degradation rule were embedded into the general package ABAQUS® through Fortran program interface. A parametric study considering geometries of joints was performed to evaluate their resultant influence on high temperature tensile behavior and the associated damage mechanisms for the CMC/superalloy double-bolt joint. New findings were provided for full exploitation of high performance through geometric design of ceramic matrix composite hot structure for hypersonic aircraft.

1. Introduction

In excursion of hypersonic vehicle, harsh high temperature flight environment poses a severe challenge to thermal protection structure and materials of aircraft. Ceramic matrix composite (CMC) materials have a series of advantages [1–4], including high specific strength and specific elastic modulus, moderate fracture toughness, and excellent oxidation resistance and heat insulation performance at high temperatures, thus becoming one of the most promising hot structural materials used for thermal protection system in hypersonic aircraft [5–7]. In the European HERMES and Hopper reusable Orbiter projects, the researchers successfully designed and manufactured C/SiC composite heat shields and heat insulation components [8]. The rear flaps of X-38 manned space shuttle used more than 400 sets of screws and nuts to assemble four ceramic matrix composite flap parts together [8]. In the developed SHEFEXII thermal protection system by DLR, Germany, ceramic matrix composite panel is connected to the primary structure of spacecraft by using rivet fastening bolts. The interior is filled with high temperature-resistant heat insulation materials. Under thermal cycle conditions, the design of connection structure has been reported to be a key issue in the

development of advanced thermal protection system used for next-generation hypersonic vehicles [9].

Take continuous carbon fiber-reinforced SiC composite materials, for example, when employing isothermal CVI technology for preparation of C/SiC composite materials, a relatively slow deposition rate was usually applied in order to prevent initial reaction sediment blocking pore channel. Under these circumstances, the fabrication cycle of C/SiC composite materials could be up to hundreds or even thousands of hours [10]. Extremely high costs caused by the complex fabrication technology have becoming increasingly prominent as the extensive application of ceramic-based composites in the aerospace field. As regard large and/or geometrically complex components, the existing fabrication approaches have certain limitations in the component size and shape, as well as in the uniformity and completeness of densification in the preparation process. How to realize the connection between composite material and small metallic parts would be of great significance for development of ceramic matrix composite key components for advanced applications. Among the developed joining techniques, mechanical joining by introduction of fasteners may overcome the shortages of existing joining techniques and improve the bearing ability and reliability of connecting parts. Advantages and disadvantages of connection will produce a direct impact on the safety and service life of vehicle structures. According to the statistics, 60%-80% of vehicle structure damage is attributed to the failure of connection parts [11], which is more prevalent in the composite connection structure. Therefore, the strength analysis and structural design of mechanical connections play a vital role in improving load-carrying efficiency and ensuring service safety of aircraft structures.

There are many factors affecting the load-bearing capacity of mechanical connection structures of composite materials. In addition to category and assembly parameters of fasteners [12–25], the number of fasteners and geometric parameters of connection structure also have a significant impact on load-bearing capacity and damage failure behavior of composite connection structure. Okutan and Karakuzu [26] experimentally and numerically characterized the failure mechanisms of Eglass epoxy laminates pinned joints, and then, they evaluated the effect of geometric dimensions on bearing, shear out, and net tension strength of the joints. The data obtained from pin-loaded laminate tests were compared with the ones calculated from a finite element model. Based on the results, they concluded that ply orientation and geometries of composites could be crucial for pinned laminated composite joints. Karakuzu et al. [27, 28] studied the effects of geometrical parameters such as the edge distance-to-hole diameter ratio (E/D), the plate width-to-hole diameter ratio (W/D), and the distance between two holes-to-hole diameter ratio (M/D) on the failure loads of woven-glass–vinylester composite plates with two serial pins, by experimental tests and numerical method. The obtained results showed that the ultimate load capacity of composite laminates with pin connections increased by increasing the values of E/D, W/D, and M/D. Kishore et al. [29] studied the mechanical behaviors of three- and four-pin joints in glass fiber/epoxy composite laminates as functions of geometric parameters, with main emphasis on pitch-to-diameter ratio. Numerical analysis was performed using a two-dimensional finite element model incorporated with Tsai-Wu failure criteria to predict damage propagation and failure load. Experiments were conducted to validate the results obtained from finite element analysis. Ozen and Sayman [30] carried out experimental and numerical studies to observe the first failure load and bearing strength of pinned joints of glass fiber-reinforced woven epoxy composite subjected to traction forces by two serial rigid pins. The edge distance-to-hole diameter (E/D), the distance between two holes-to-hole diameter (M/D), and the distance from the upper or the lower edge of the specimen to the center of hole-to-hole diameter (K/D) ratios were selected as parameters to evaluate their influences on failure mode, failure load, and bearing. Tang et al. [31] studied the mechanical property and failure mechanism of carbon–carbon braided composites (C–Cs) single-bolt and double-bolt (SBS and DBS) joints structure subjected to unidirectional tensile load by experimental method and numerical analysis. It was found that the dominant failure modes for both *C–Cs* SBS and DBS joint configurations were bearing failure and net tension. After comparison of experimental observations and simulation results, parametric studies were implemented by using finite element analysis to classify the effects of geometric parameters including joint width (W), edge distance (e), and bolt pitch (p) on the SBS and DBS joint configurations. Li et al. [24, 32] provided a new joining technology for C/SiC composites and investigated the influence of drilling holes, hole distribution (including ratios of edge distance to diameter (E/D), width to diameter (W/D), and hole distance to diameter (H/D)), and number of applied pins on the mechanical properties of C/SiC substrates and joints. The testing results showed that drilling holes and hole distribution greatly affect the mechanical properties of C/SiC substrates, but when adopting an optimized principle, the effect could be neglected. With the increase of pins, the reliability of joints was improved, and the fracture mode changes from interlayer damage to substrate rupture. In spite of the above-mentioned research in the literatures, little attention was paid on mechanical behavior of CMC joining at elevated temperatures, especially the influence of geometric dimensions of applied fasteners on the mechanical properties and damage failure modes of C/SiC joints under the corresponding circumstances.

To address the above concerns, a 3D finite element model coupled with progressive damage analysis is firstly carried out to predict high temperature tensile properties and failure behavior of single-lap, double-bolt CMC/superalloy hybrid joints. A macroscopic phenomenological constitutive model is employed to describe the nonlinear stress-strain behavior of 2D plain-woven C/SiC composites. Damage accumulations in the composite laminates are evaluated by using Alvaro's failure criteria combined with the Tan's property degradation model. A parametric study considering geometries was performed to evaluate their resultant influence on high temperature tensile behavior and damage mechanisms for the studied double-bolt hybrid joint.

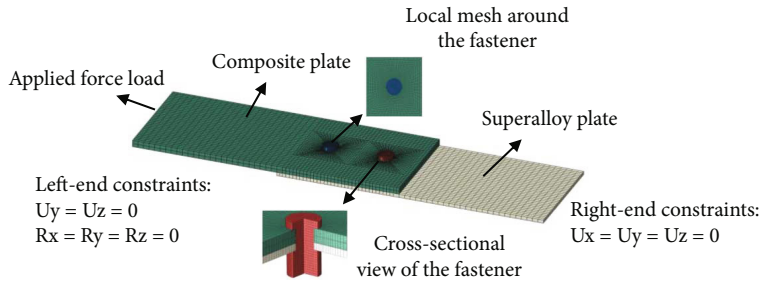

Figure 1: Finite element model of the 2D C/SiC composite-superalloy double bolted joint configuration.

Table 1: Material types and structural parameters of the studied C/SiC composite and superalloy double bolted joint.

Parameters	Value
Length of 2D woven C/SiC composite plate	120 mm
Width of 2D woven C/SiC composite plate	50 mm
Thickness of 2D woven C/SiC composite plate	3 mm
Length of GH4169 superalloy plate	120 mm
Width of GH4169 superalloy plate	50 mm
Thickness of GH4169 superalloy plate	1.5 mm
Laping length	50 mm
Plate margin distance	15 mm
Double-bolt center spacing	25 mm
Diameter of bolt made of GH4141 alloy	5 mm

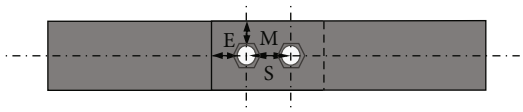

Figure 2: Schematic diagram of the geometry parameters of the studied double bolted joints for the parametric study.

2. Finite Element Modeling

To simulate the high temperature tensile properties and their associated damage modes of single-lap, double-bolt 2D C/SiC composite and superalloy joint assembled by two serial protruding head bolts, an finite element model is established to mimic quasi-static unidirectional tensile loading of the hybrid bolted joint via ABAQUS/standard software, as illustrated in Figure 1. The material types and structural parameters for the CMC/superalloy double bolted joint are shown in Table 1. The experimental stress-strain curves upon uniaxial tension and shear loads and the rest of mechanical properties of 2D plain-woven C/SiC composite material as well as the assigned high temperature mechanical properties of the superalloy materials used for analysis have been provided in Ref. [33, 34]. Three-dimensional eight-node reduced integration C3D8R elements with hourglass control were used to discretize the composite laminates, superalloy plate, and mechanical fastener. In order to improve computational efficiency, hexagonal heads for bolt and nut were simplified as round heads, and the bolt and nut were modeled as entirety to decrease contact surfaces. Ten contact pairs for the joint structure were defined between fastener shanks and holes of plates, fastener heads or nuts and the outer surfaces of the two plates, and the faying surfaces of two plates. A finite sliding contact and surface to surface contact formulations were adopted between all contact interfaces in the model. A classic Coulomb friction was assigned to all contacted surfaces with friction coefficient of 0.3. Bolt-hole clearance value 3% was set to the joint through setting interference fit values of the contact pairs between fastener shank and holes in two plates. A 6 kN preload was applied for all the considered joints through Bolt load function in ABAQUS. The right end of superalloy plate was held fixed in all three translational directions (Ux, Uy, and Uz). The left end of the composite plate was held fixed in two translational directions (Uy and Uz) and three rotational directions (Rx, Ry, and Rz), while a uniform force load was applied along Ux direction to mimic a quasi-static tensile loading. The uniform temperature loads of 25°C, 150°C, 300°C, 450°C, 600°C, and 750°C were, respectively, imposed to the entire joint structures to examine the temperature-dependent behavior of mechanical properties of the joints. To gain further insight into effect of geometric dimensions of the double bolted joints, the edge distance (E), plate margin distance (M), and double-bolt center spacing (S) of the joint, as schematically shown in Figure 2, will be selected for parametric studies on the mechanical behaviors of the CMC/superalloy double bolted joints at elevated temperatures.

3. Progressive Damage Analysis Method

3.1. Nonlinear Stress-Strain Constitutive Relationship Containing Composite Damage. The damage process of composite material is a progressive and irreversible process with material strength and stiffness degradation, deformation, and energy dissipation under the action of external load and/or environmental effects. This process can be divided into stages: damage initiation, damage progression, local damage, and final fracture damage. The study of failure mechanism of ceramic matrix composites is mainly based on emerge and evolution of cracks within materials and further explores the influence of crack nucleation and propagation on the macroscopic mechanical properties.

If the composite material is in the linear elastic deformation range, the relationship between stress $\widehat{\sigma}$ and strain $\widehat{\varepsilon}$ is given as:

$$\widehat{\sigma} = \mathrm{C}_0 : \widehat{\varepsilon}, \tag{1}$$

where C_0 represents the linear elastic stiffness matrix of the composite and can be determined from material engineering modulus by the linear elasticity theory [35].

As the damage occurs within the composite material, the material stiffness gradually degenerates with the damage propagation and accumulation. Define $d_i \in [0, 1], i = 1, 2, \cdots, 6$, where the stiffness damage coefficient d_i=0 represents damage-free and d_i=1.0 represents full damage. And then, the damage factor tensor of composites can be introduced as:

$$M = \mathrm{diag}\left[\frac{1}{\sqrt{1-d_1}}, \frac{1}{\sqrt{1-d_2}}, \cdots, \frac{1}{\sqrt{1-d_6}}\right]. \tag{2}$$

Establish the relationship between the linear elastic stress $\widehat{\sigma}$ and the actual stress σ:

$$\widehat{\sigma} = M : \sigma. \tag{3}$$

According to the elastic strain energy equivalence principle by Sidoroff [36], it is assumed that the strain energy of damaged composite equals the quantity of original composite. The relationship between the damage stiffness matrix C and C_0 is expressed as:

$$C = M^{-1} : C_0 : \left(M^T\right)^{-1}. \tag{4}$$

The nonlinear stress-strain relationship of the damaged composite with orthogonal anisotropic feature is given:

$$\begin{Bmatrix} \sigma_1 \\ \sigma_2 \\ \sigma_3 \\ \tau_{12} \\ \tau_{13} \\ \tau_{23} \end{Bmatrix} = \begin{Bmatrix} C_{11} & C_{12} & C_{13} & 0 & 0 & 0 \\ C_{12} & C_{22} & C_{23} & 0 & 0 & 0 \\ C_{13} & C_{23} & C_{33} & 0 & 0 & 0 \\ 0 & 0 & 0 & C_{44} & 0 & 0 \\ 0 & 0 & 0 & 0 & C_{55} & 0 \\ 0 & 0 & 0 & 0 & 0 & C_{66} \end{Bmatrix} \begin{Bmatrix} \varepsilon_1 \\ \varepsilon_2 \\ \varepsilon_3 \\ \gamma_{12} \\ \gamma_{13} \\ \gamma_{23} \end{Bmatrix}, \tag{5}$$

where:

$$\begin{cases} C_{11} = (1-d_1)C_{11}^0, C_{44} = (1-d_4)C_{44}^0 \\ C_{22} = (1-d_2)C_{22}^0, C_{55} = (1-d_5)C_{55}^0 \\ C_{33} = (1-d_3)C_{33}^0, C_{66} = (1-d_6)C_{66}^0 \\ C_{11} = \sqrt{(1-d_1)(1-d_2)}C_{12}^0 \\ C_{13} = \sqrt{(1-d_1)(1-d_3)}C_{13}^0 \\ C_{23} = \sqrt{(1-d_2)(1-d_3)}C_{23}^0 \\ \varepsilon_1 = \varepsilon_{11} - \alpha_1 \Delta T \\ \varepsilon_2 = \varepsilon_{22} - \alpha_2 \Delta T \\ \varepsilon_3 = \varepsilon_{33} - \alpha_3 \Delta T \end{cases}, \tag{6}$$

where ε_{11}, ε_{22}, and ε_{33} and γ_{12}, γ_{13}, and γ_{23} represent the actual strain under the material coordinate system; α_1, α_2, and α_3 represent the linear expansion coefficient in the three main directions of composite material; and ΔT represents the temperature difference between actual temperature and reference temperature of composite material element.

Carbon fiber-reinforced SiC ceramic matrix composite materials exhibit nonlinearity and pseudo-plasticity due to damage of matrix cracks, interface slipping and debonding, fiber failure and fiber pull-out under uniaxial tensile, and shear loading [37]. The damage progression will dissipate energy of external load and reduce the stiffness of material. To address the nonlinear stress-strain behavior of CMC materials, a macroscopic constituent model proposed by Li [38] is adopted in the present study to characterize the mechanical behavior of 2D plain-woven C/SiC composite materials. Their model will be described here briefly. The experimental stress-strain relationships upon uniaxial tensile and shear loading for the material are fitted with five-order polynominal function. And then, first-order derivative of the tangent modulus with respect to the detectable strain was found according to the fitted stress-strain relationship upon tensile and shear loading.

$$\begin{aligned} \mathrm{E}_i^{\tan} &= \frac{d\sigma_i}{d\varepsilon_i} = A_1 + 2A_2\varepsilon_i + 3A_3\varepsilon_i^2 + 4A_4\varepsilon_i^3 + 5A_5\varepsilon_i^4 \left(0 \le \varepsilon_i \le \varepsilon_i^f, i = 1, 2\right), \\ G_{12}^{\tan} &= \frac{d\tau_{12}}{d\gamma_{12}} = B_1 + 2B_2\gamma_{12} + 3B_3\gamma_{12}^2 + 4B_4\gamma_{12}^3 + 5B_5\gamma_{12}^4 \left(|\gamma_{12}| \le \gamma_{12}^f\right), \end{aligned} \tag{7}$$

where ε_i^f is the tensile fracture strain, γ_{12}^f is the shear fracture strain in the 1-2 plane, and A_j and $B_j (j = 1, 2, .., 5)$ are the fitted coefficients. When the tensile strain ε_i and shear strain γ_{12} equal zero, the $E_i^{\tan}$ and $G_{12}^{\tan}$ are the initial elastic modulus E_1^0 and shear modulus G_{12}^0 of the C/SiC composite.

Under tensile and shear unloading or reloading processes, the elastic modulus E_1^u and shear modulus G_{12}^u can be fitted by using a logical function with the associated strain

as given:

$$\begin{aligned} \mathrm{E}_i^u &= A_6 + \frac{A_7 - A_6}{1 + (\varepsilon_i^m / x_0)^{p_0}} (\varepsilon_i \le \varepsilon_i^m, i = 1, 2), \\ \mathrm{G}_{12}^u &= B_6 + \frac{B_7 - B_6}{1 + (|\gamma_{12}^m| / x_1)^{p_1}} (|\gamma_{12}| \le |\gamma_{12}^m|), \end{aligned} \tag{8}$$

where A_6, A_7, p_0, x_0, and B_6, B_7, p_1, and x_1 are the shape parameters of each logical function.

The stress and strain responses of composites under compressive loading are approximate to linear elastic relation, and the selection of compressive modulus is divided into two circumstances. When the stress level of the material exceeds a microcrack closure point C $(\varepsilon^r, \sigma^r)$, closure of the microcracks leads partially to recovery of initial elastic property E_i^0. Otherwise, the compressive modulus is the same as the unloading modulus in tensile loading and unloading curve.

$$\begin{cases} \sigma_i = E_i^0 \varepsilon_i & \left(\varepsilon_i \ge \varepsilon_i^b, \sigma_i \le \sigma_i^r, i = 1, 2\right) \\ \sigma_i = E_i^u \varepsilon_i & \left(\sigma_i^r \le \sigma_i \le 0, i = 1, 2\right) \end{cases}, \tag{9}$$

where ε_i^c is the compressive fracture strain and σ^r is the stress at the microcrack closure point C.

3.2. Failure Criterion. Different from other types of composites, both fibers and matrix of ceramic matrix composites are generally brittle materials, which will produce cracks in the composites upon external loading. The initiation and propagation of cracks will eventually lead to failure of composite material. The damage mechanisms of fiber-reinforced ceramic matrix composites mainly include matrix microcrack, interface debonding, fiber pull-out and fracture, crack bifurcation, crack bridging, and crack deflection. When numerical method is used to simulate the progressive damage accumulation of composite materials, a corresponding composite damage criteria are applied to judge the damage failure of material elements. Many scholars have proposed different forms of failure criteria to determine composite damage, such as maximum stress criterion [25], maximum strain criterion [39], Tsai-Wu criterion [25, 40, 41]], and Hashin failure criterion [42]. Alvaro [43] extends the two-dimensional Chang-Lessard failure criterion to three dimensions and incorporates the effects of fiber-matrix shear failure to justify the occurrence of relevant failure modes. The proposed criterion by Alvaro can examine the fiber failure in tension and compression, matrix cracking in tension and compression, fiber-matrix shear out failure, and fiber-matrix interlaminar tension and compression failures. The three-dimensional Alvaro failure criterion is specifically expressed as follows:

Matrix tensile failure ($\sigma_{22} \ge 0$):

$$\left(\frac{\sigma_{22}}{Y_t}\right)^2 + \left(\frac{\tau_{12}}{S_{12}}\right)^2 + \left(\frac{\tau_{23}}{S_{23}}\right)^2 \ge 1. \tag{10}$$

Matrix compression failure ($\sigma_{22} < 0$):

$$\left(\frac{\sigma_{22}}{Y_c}\right)^2 + \left(\frac{\tau_{12}}{S_{12}}\right)^2 + \left(\frac{\tau_{23}}{S_{23}}\right)^2 \ge 1. \tag{11}$$

Fiber tensile failure ($\sigma_{11} \ge 0$):

$$\left(\frac{\sigma_{11}}{X_t}\right)^2 + \left(\frac{\tau_{12}}{S_{12}}\right)^2 + \left(\frac{\tau_{13}}{S_{13}}\right)^2 \ge 1. \tag{12}$$

Fiber compression failure ($\sigma_{11} < 0$):

$$\left(\frac{\sigma_{11}}{X_c}\right)^2 \ge 1. \tag{13}$$

Fiber-matrix shear out failure ($\sigma_{11} < 0$):

$$\left(\frac{\sigma_{11}}{X_c}\right)^2 + \left(\frac{\tau_{12}}{S_{12}}\right)^2 + \left(\frac{\tau_{13}}{S_{13}}\right)^2 \ge 1. \tag{14}$$

Tensile delamination failure ($\sigma_{33} \ge 0$):

$$\left(\frac{\sigma_{33}}{Z_t}\right)^2 + \left(\frac{\tau_{13}}{S_{13}}\right)^2 + \left(\frac{\tau_{23}}{S_{23}}\right)^2 \ge 1. \tag{15}$$

Compression delamination failure ($\sigma_{33} < 0$):

$$\left(\frac{\sigma_{33}}{Z_c}\right)^2 + \left(\frac{\tau_{13}}{S_{13}}\right)^2 + \left(\frac{\tau_{23}}{S_{23}}\right)^2 \ge 1. \tag{16}$$

3.3. Material Degradation Model. In progressive damage analysis of composite materials, the composite continues to bear the load, even with local damage occurring inside the composite laminate. Once the damage initiates, the most commonly used method is to reduce stiffness of the "failed" elements and then redistribute the load with nearby elements while maintaining a global equilibrium. Material property degradation model is utilized to describe the equivalent material stiffness characteristics of failure regions. Researchers have put forward many rules of material performance degradation, mainly divided into two categories: sudden degradation model and continuous degradation model. The sudden degradation model assumes that the macroscopic damage occurs and runs through the whole elements when the strain state of material meets the failure criteria. The material properties instantly degenerate into part of their values before failure. The advantage of this method is easy to be implemented and converged in numerical calculation. However, the ultimate load-bearing capacity of composites would be overestimated in comparison with the data in the actual situation of material failure. The second method is a continuous degradation model, where the stiffness attribute of composites is a continuous function of strain variable. Since the material mechanical behavior is often nonlinear, the stiffness degradation coefficient will change with the strain level. In spite of highly computational task and poor convergence, the simulated results by this

Table 2: Tan's material degradation model.

Damage mode	Tan's rule
Matrix tensile failure	$E_{22} \longrightarrow 0.2E_{22}, G_{12} \longrightarrow 0.2G_{12}, G_{23} \longrightarrow 0.2G_{23}$
Matrix compression failure	$E_{22} \longrightarrow 0.4E_{22}, G_{12} \longrightarrow 0.4G_{12}, G_{23} \longrightarrow 0.4G_{23}$
Fiber tensile failure	$E_{11} \longrightarrow 0.07E_{11}$
Fiber compression failure	$E_{11} \longrightarrow 0.07E_{11}$
Fiber-matrix shear out failure	$G_{12} = \nu_{12} = 0$
Tensile delamination failure	$E_{33} = G_{23} = G_{13} = \nu_{23} = \nu_{13} = 0$
Compression delamination failure	$E_{33} = G_{23} = G_{13} = \nu_{23} = \nu_{13} = 0$

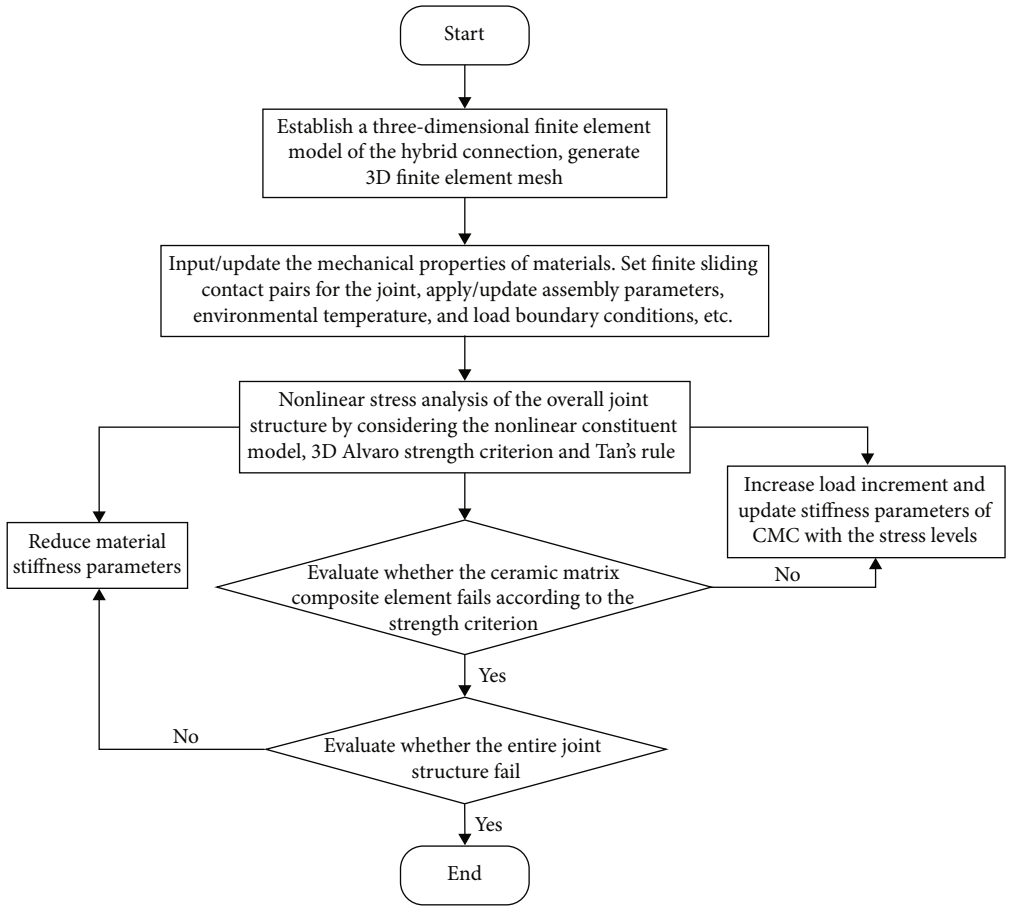

Figure 3: Flowchart for progressive damage analysis of the hybrid joint with two series bolts.

approach are closer to the actual simulation situation. In this study, a continuous degradation model proposed by Tan [44], as specifically shown in Table 2, will be used to reduce the stiffness of "failed" elements of composites.

3.4. Analysis Procedure and Validation of the Progressive Damage Model. To implement a progressive failure analysis of *C*/SiC composite and superalloy double bolted joint, a user-defined subroutine UMAT including the nonlinear constitutive model, 3D Alvaro failure criterion and Tan's material degradation rule were embedded into the general package ABAQUS® through Fortran program interface. In this subroutine, the predefined field variables were described as functions of material properties, which were then used for mechanical behavior expression of any material point. Figure 3 demonstrates the flowchart for progressive damage analysis of the hybrid joint with two series bolts. The basic progressive damage analysis steps are as follows:

(1) According to the geometric configuration of the ceramic matrix composite and superalloy double bolted joint, a three-dimensional finite element model of the hybrid connection structure is established

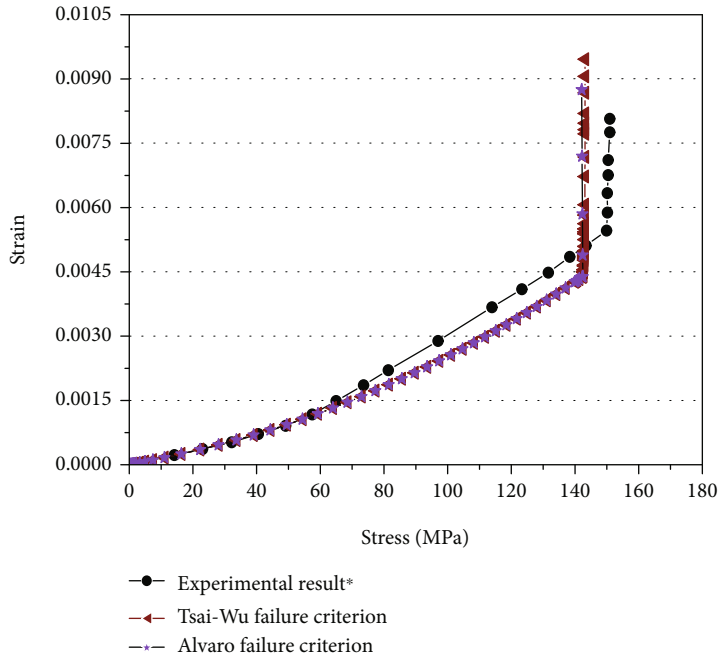

Figure 4: Comparison of simulated tensile stress and strain relationship by using Tsai-Wu and 3D Alvaro failure criteria with experimental results in Li et al. [33] for 2D plain-woven C/SiC composite open-hole plate.

(2) Input/update the mechanical properties of the 2D plane-woven C/SiC composite and superalloy materials. Apply/update parameters such as the assembly clearance and pretightening force, environmental temperature, and load boundary conditions to the finite element model

(3) Nonlinear stress analysis is carried out on the overall joint structure by considering the nonlinear behavior of ceramic matrix composite and the elastic behavior of superalloy material

(4) The calculated stress at each element is substituted into the 3D Alvaro strength criterion to evaluate whether the ceramic matrix composite element fails

(5) If the failure criterion is violated, the applied load is increased by a load increment and the stiffness parameters for CMC are updated in accordance with the obtained stress levels, go to step 2. Otherwise, judge whether the final structure failure is satisfied

(6) If the final failure is not achieved, the material stiffness parameters are reduced according to the Tan's rule for the C/SiC composite, and stress analysis of the entire joint structure is carried out at the next load increment level from the step 2

(7) The simulation is terminated until encountering final failure of the composite structure or severe convergence difficulties

The nominal stress-strain curves of an open-hole 2D plain-woven C/SiC composite laminate under uniaxial tensile loading were simulated according to the geometric configuration and test conditions of composite specimen given in the Reference [36]. Comparison of simulated tensile stress and strain relationship by using Tsai-Wu and 3D Alvaro failure criteria with experimental results in Li [38] for 2D plain-woven C/SiC composite open-hole plate is shown in Figure 4. As can be seen from the figure, the slope in elastic stage from the simulated stress-stain curves of the specimen by using Tsai-Wu and Alvaro failure criteria agrees with the experimental data. However, the predicted stiffness of the composite laminates in damage stage is below the experimental value, possibly due to the SiC antioxidant coating deposited on the experimental specimen surface in tests. The failure stress of the open-hole composite laminate by using Tsai-Wu and Alvaro failure criteria were, respectively, 143.1 MPa and 142.1 MPa, very close to the experimental ultimate stress 149.9 MPa. However, the simulated fracture strain of the open-hole composite by 3D Alvaro failure criteria is in accordance with the experimental result within 8.4%, fitting better than the data 17.2% by using Tsai-Wu criteria. This simulation error level validates the effectiveness of the proposed progressive failure model in the present research.

4. Results and Discussions

4.1. High Temperature Mechanical Behaviors of the Studied Joints. The tensile performances of the hybrid CMC/superalloy double bolted joint were simulated under various temperature levels by using the established progressive damage analysis method. The predicted load-displacement curves upon tensile loading of the mechanically fastened joints are illustrated in Figure 5. As can be clearly seen from the Figure 5, at the temperatures of interest, the slope of curves shows declining trend, which means that the initial stiffness

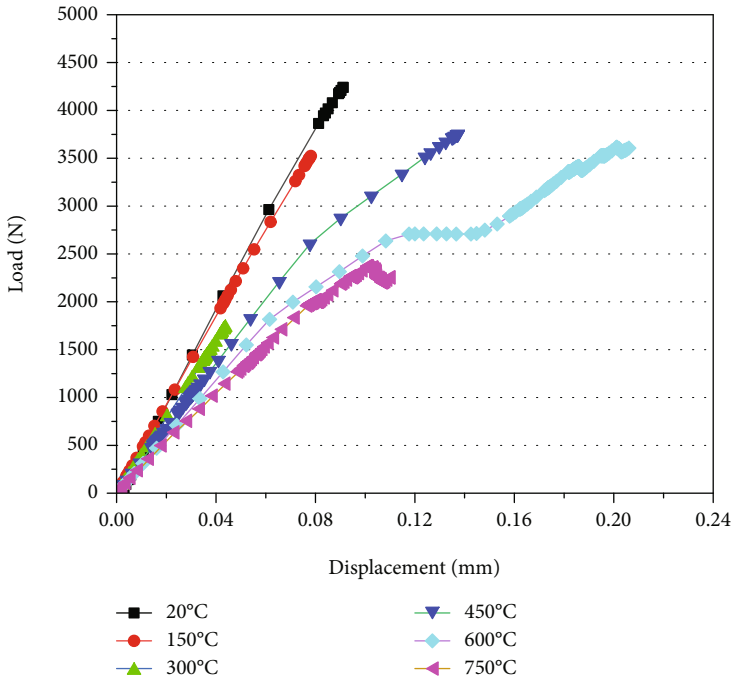

Figure 5: Load–displacement relationships for the C/SiC composite and superalloy double bolted joints under various levels of environment temperature.

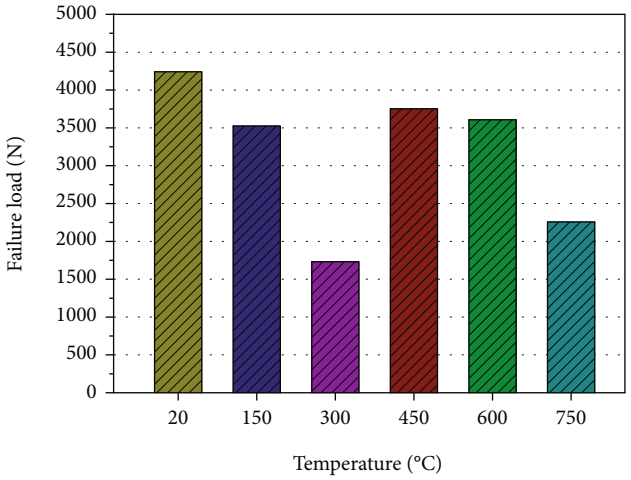

Figure 6: Variation of the maximum failure load with respect to environment temperature for the studied CMC/superalloy double bolted joint.

of the hybrid bolted joints drops with the rise of applied temperature. The stiffness reduction is mainly due to the fact that the continuous preload relaxation upon temperature rising lessens the friction force on the contact surface of two plates, which is used for resisting the external tensile load, as we discussed in previous research [34]. Variation of the maximum failure load with respect to environment temperature for the studied CMC/superalloy double bolted joint is shown in Figure 6. Figure 7 demonstrates damage failure patterns around the inner fastener hole of ceramic matrix plate of the double bolted joints at various temperatures for consideration. The simulation damage failure patterns of FEM elements demonstrate that all failures are taken place at the inner fastener hole of ceramic matrix plate at various temperatures, as shown in Figure 6. For the considered joint geometry and assembly conditions, the maximum failure load 4241 N takes place at room temperature. The failure load of the hybrid joint structure gradually declines with the applied environment temperature at temperatures below 300°C, reaching the minimum value of 1731 N at 300°C. In this temperature range, a small drop in the pretightening force of the joint structure was taken place, and the main failure mode is compression delamination failure of CMC elements around the CMC hole edge. At 300°C-450°C, the high temperature environmental effect leads to a continuous increase in the shear stress of ceramic matrix composite, fiber-matrix shear failure, and compression delamination failure occur within the CMC laminates, and the failure load of joint structure increases rapidly. With a further temperature increase, matrix compression failure, fiber compression failure, fiber-matrix shear failure, and compression lamination failure exist around the CMC hole edge at 600°C. As the temperature reaches 750°C, the compression delamination failure does not occur due to significant reduction in the pretension force, and the final failure modes become matrix compression failure, fiber compression failure, and fiber-matrix shear failure. The damage area is expanding compared to the results at 600°C, and the failure load drops further from 3607 N at 600°C to 2254 N at 750°C under the combination of multiple failure modes. As discussed in our previous research on single bolted joint structure of CMC and superalloy plates, the thermal expansion mismatch generated between the CMC and superalloy materials led to significant changes in the assembly preload

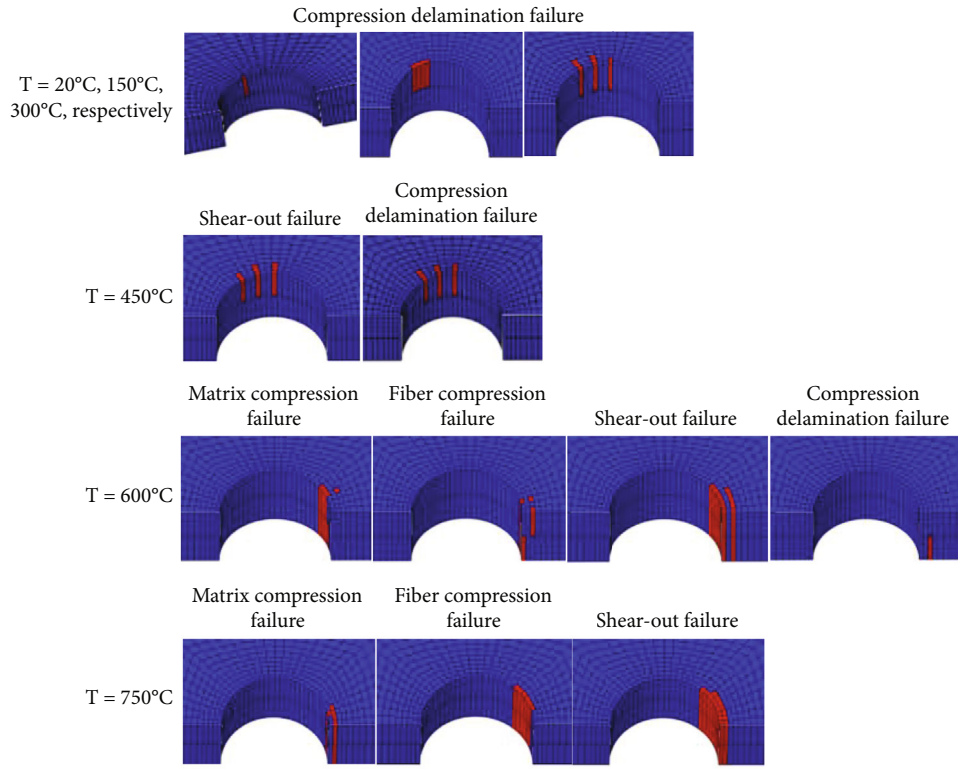

Figure 7: Damage failure patterns around the inner fastener hole of ceramic matrix plate of the double bolted joints at various temperatures.

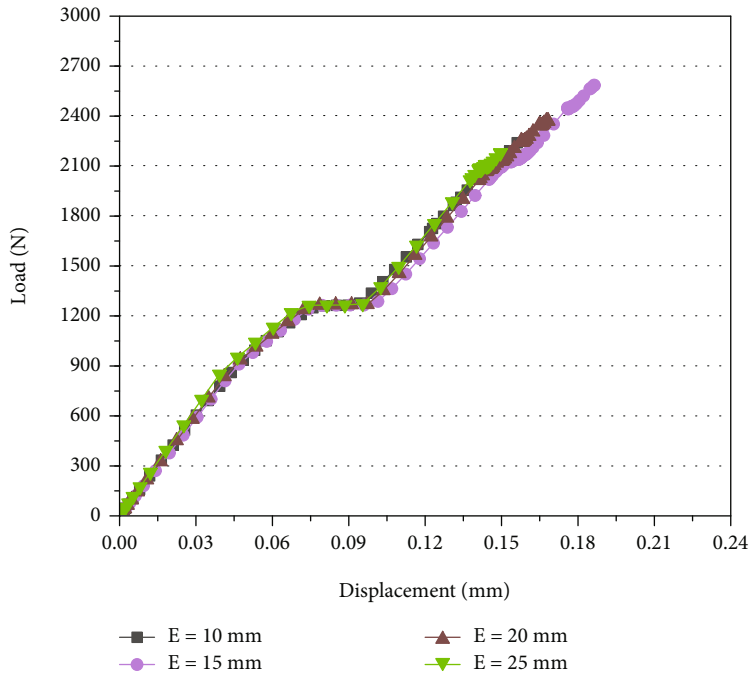

Figure 8: Load–displacement relationships for the C/SiC composite and superalloy double bolted joints under various levels of edge distances at 750°C.

and bolt-hole clearance as the temperature load is applied to the joint. There exists an optimal match in the initial assemble parameters to maximize or minimize the load-bearing capacity of the joint structure at each temperature or at the whole reference temperature range. As a result, the ultimate failure load of the studied hybrid CMC/superalloy double bolted joint exhibits the above diverse trend with respect to the environment temperature.

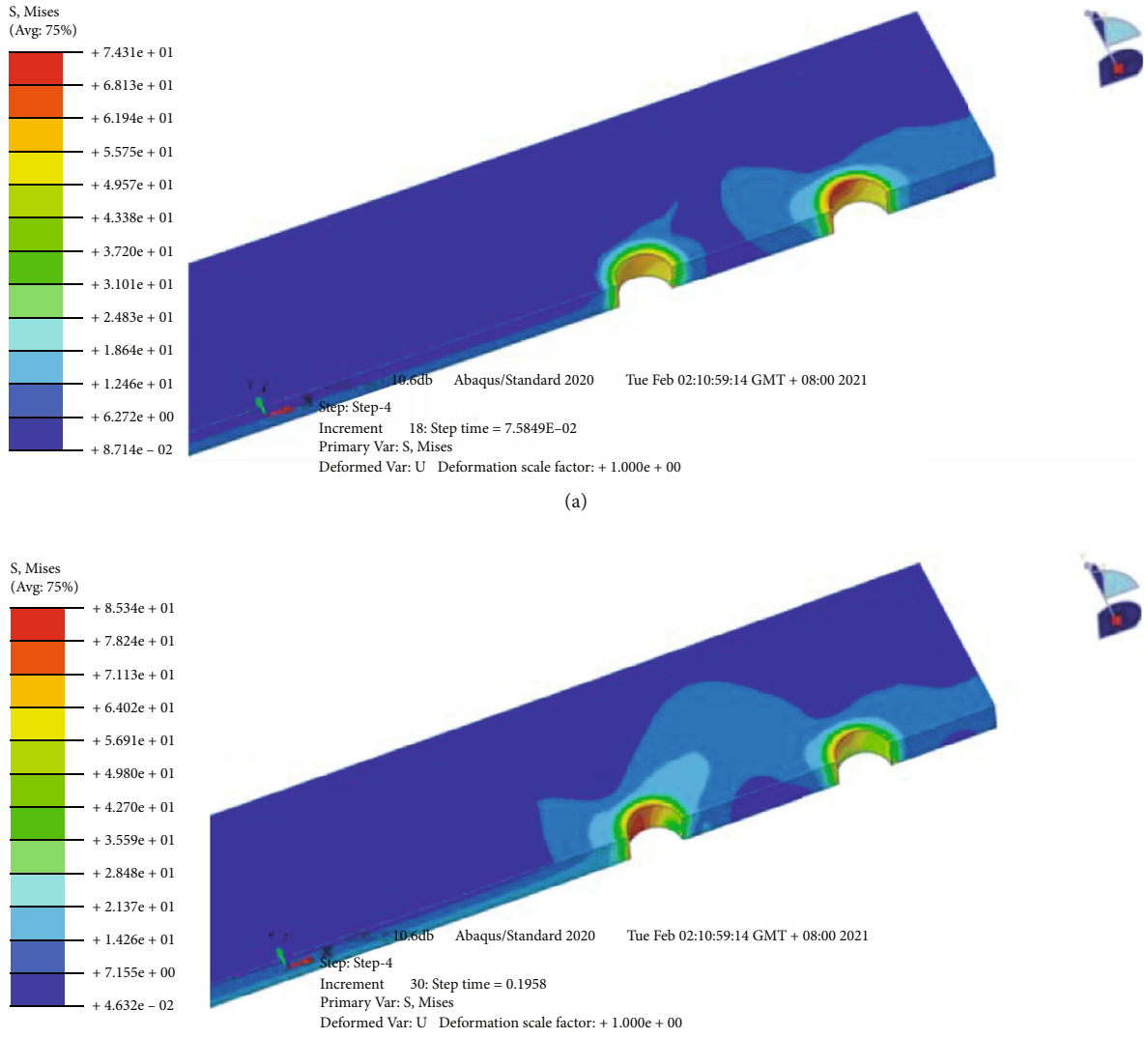

Figure 9: Mises stress contour maps of the ceramic matrix composite plate for the studied joint with 10 mm edge distance at the applied loading levels of 700 N (a) and 1250 N (b) at 750°C.

4.2. Effect of the Edge Distance of Joints. To study the influence of edge distance on mechanical performances of the C/SiC CMC and superalloy double bolted joint, the load-displacement curves of the joints with different edge distances upon uniaxial static tensile loading conditions are simulated at 750°C, and the predicted results for the joints are shown in Figure 8. From the figure, it can be observed that the loading displacements reach around 0.07 mm, and there appears horizontal section in their load-displacement curves of joints with all considered edge distances. This section can be explained from the stress cloud map example of ceramic matrix composite plate with 10 mm edge distance at the applied load levels of 700 N and 1250 N, as shown in Figure 9. In tensile loading process of the joint, the maximum stress around the outer hole of the ceramic-based composite plate is greater than that of the inner one at 700 N tensile load. As the tensile displacement continues to increase, the Mises stress around the outer hole gradually decreases, whereas the stress around the inner hole increases, indicating that the tensile load is transmitted from the outer bolt to the inner one in tensile loading process. Since there is a certain clearance between bolt shank and ceramic-based composite hole, the structural tensile load does not vary as the tensile displacement of the connection structure increases at the applied load level of 1250 N tensile load. In the present study, when the edge distance of double bolted connection structure is constantly increasing, the stiffness of the joint is hardly changed at 750°C. However, the high temperature failure load increases first and then decreases with the structural edge distance, varying from 2177.7 N to 2585.2 N, as shown in Figure 10. The structure failure load reaches the maximum value as the structure edge distance is 15 mm. Ozen and Sayman [30] carried out an experimental and numerical study to investigate the first failure load and bearing strength behavior of two serial pinned joints of glass fiber-reinforced woven epoxy composite at room temperature. Their results demonstrated that high values of edge distance-to-hole diameter (E/D) ratios

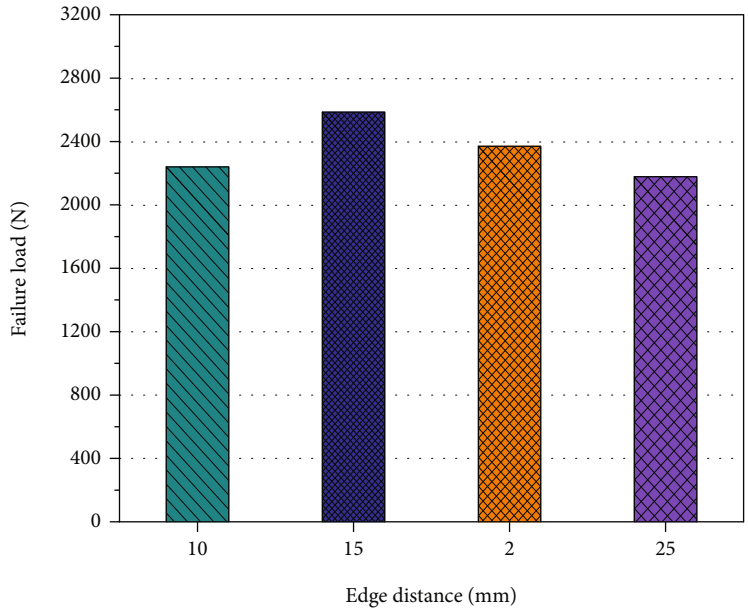

Figure 10: Variation of the failure load with edge distance for the studied CMC/superalloy double bolted joints at 750°C.

improve the failure load of the pinned joints. Karakuzu et al. [27, 28] investigated the effects of geometrical parameters on failure loads and failure modes in woven-glass–vinylester composite plates with two serial pin-loaded holes. It was found that the failure load values are highly depending on the edge distance-to-hole diameter ratio (E/D). As the plate width-to-hole diameter ratio (W/D) and the distance between two holes-to-hole diameter ratio (M/D) are constant, the failure load increases with increasing E/D. Failure load values show small differences for specimens having $E/D > 2$. The shear out failure modes are directly related to E/D. For $E/D = 1$, failure mode is shear out. The failure modes of the specimens which have $E/D > 1$ and $M/D > 2$ are bearing failure. Tang et al. [31] studied the mechanical property and failure mechanism of carbon–carbon braided composites (C–Cs) single-bolt and double-bolt joints structure subjected to unidirectional tensile load by the experimental method and numerical analysis. They found that the failure load of the single bolted joint structure increases first with the e/D (the ratio of the distance between free edge of plate (e) and center of its hole to hole diameter (D)) until it reaches the critical value of 3.5, and then, the connection structure failure loading decreases slightly. The possible reason can be attributed to the fact that the area clamped by the bolt was enlarged with the increase of e/D, while the friction and total clamp force remain at the same original level. The bolt clamp efficiency is reduced, and thus, the failure load decreases slightly [45]. As a result, the damage failure mode of the SBS joint will change from shear failure to bearing failure at the threshold value of $e/D = 3.5$. Analogous to the 3D C-C single bolted joint, the failure loading of the double bolted joint increases with the increase of e/D, and the failure mode is a tension failure either at low or high e/D ratios. The edge distance (e) has a small influence on the stresses on shear failure plane, bearing failure plane, and tension failure plane of the DBS joint structure. The tension stress is the highest, and the failure mode is tensile failure. The variation trend of ultimate failure load with respect to the edge distance for the studied joint at 750°C seems to be in agreement with the previous conclusions made at room temperature for composite joints by Tang et al. [31]. This study also finds that changes of failure load of the joint at 750°C are mainly caused by decay of bolt tightening efficiency. The increase of edge distance will change stress concentration at hole edge of ceramic matrix composite, leading to a small change in bearing capacity of the joint structure. For the considered edge distance levels, the failure mechanisms of the CMC/superalloy double bolted joints include a small amount of matrix compression failure, most of fiber compression failure and fiber-matrix shear failure mode at temperature of 750°C.

4.3. Effect of the Plate Margin Distance of Joints. The effect studies of plate margin distance on high temperature mechanical performance of 2D C/SiC ceramic matrix composite and superalloy double bolted joints were carried out by setting the rest of geometric parameters and assemble variables of the joints as constants. The simulated load-displacement profiles of the joints with different plate margin distances at 750°C are shown in Figure 11. The relationship between high temperature failure load and the plate margin distance of joints for the considered situations is plotted in Figure 12. As can be observed from the Figures 11 and 12, the plate margin distance has weak impact on failure load of the joint structure at 750°C. Larger plate margin distance of the joint results in slight increase of the connection stiffness, mainly due to the fact that the friction between ceramic-based composite plate and superalloy plate needing to be overcome is greater as the plate margin distance is larger at the same tensile load. Ozen and Sayman [30] found that larger plate width and hole diameter ratio (W/D) can improve the load-bearing capacity of the single-

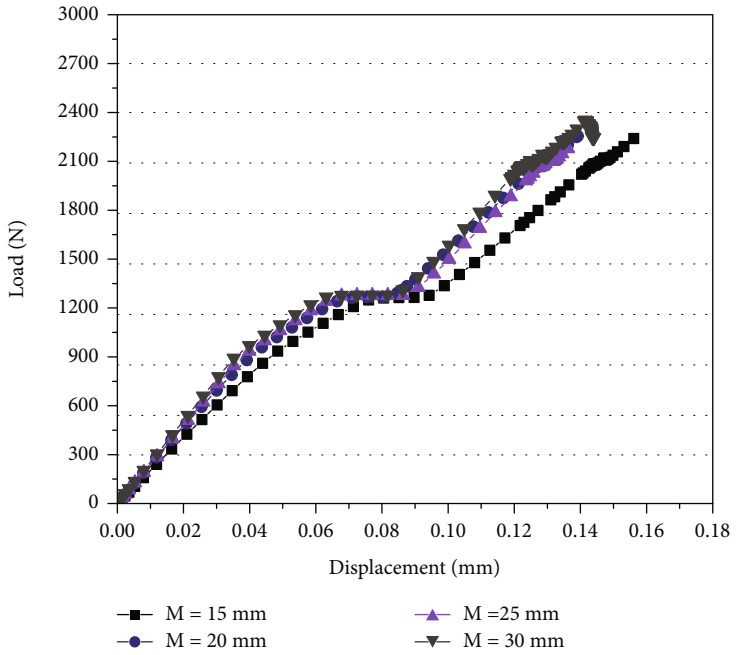

Figure 11: Load–displacement relationships for the C/SiC composite and superalloy double bolted joints under various levels of plate margin distance at 750°C.

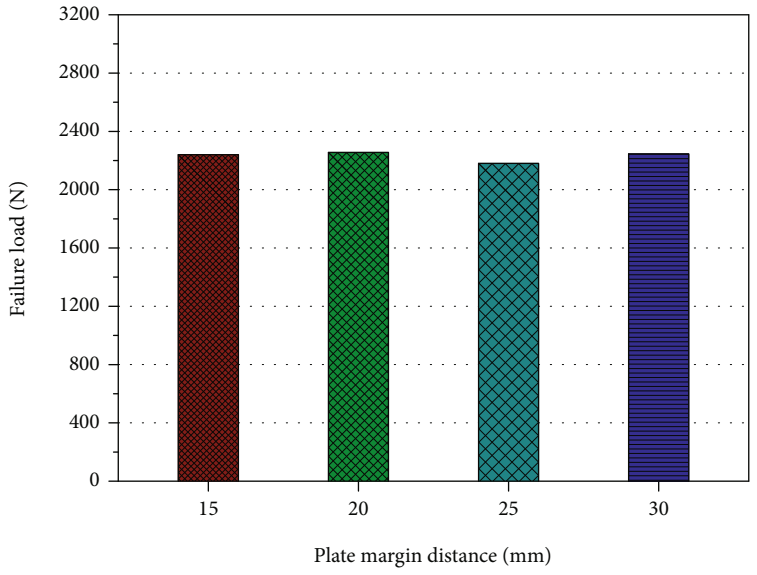

Figure 12: Variation of the failure load with plate margin distance for the studied CMC/superalloy double bolted joint at 750°C.

bolt single-lap glass fiber-epoxy composite bolt joints. Karakuzu et al. [27, 28] reported that the failure load increases with increasing plate width-to-hole diameter ratio (W/D), when the two bolts of composite joint are series mode. The damage mode of the specimen is tensile failure for the structure with small W/D. Since the tensile damage is disastrous, the W/D in series should be no less than 3. Effect studies of plate width on mechanical property of carbon–carbon braided composites (C–Cs) single-bolt and double-bolt joints structure subjected to unidirectional tensile load by Tang et al. [31] showed that the failure loading of both the single and double bolted joints increases with the increase of W/D and the failure modes change from tension failure to bearing failure at a critical value of W/D. The stress variations on failure planes with the value of W/D demonstrated that stress on the shear failure plane increases, which is always lower than the bearing stress. This implies that increase of width (W) can cause a slight enhancement of the bearing stress but a significant decrease of the tension stress. The failure mode changes from the tension failure

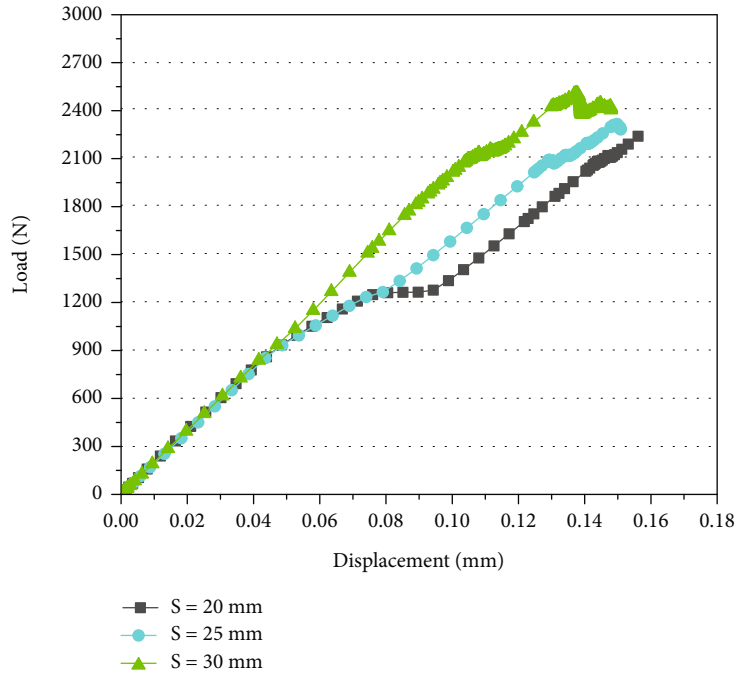

Figure 13: Load–displacement relationships for the C/SiC composite and superalloy double bolted joints under various levels of double-bolt center spacing at 750°C.

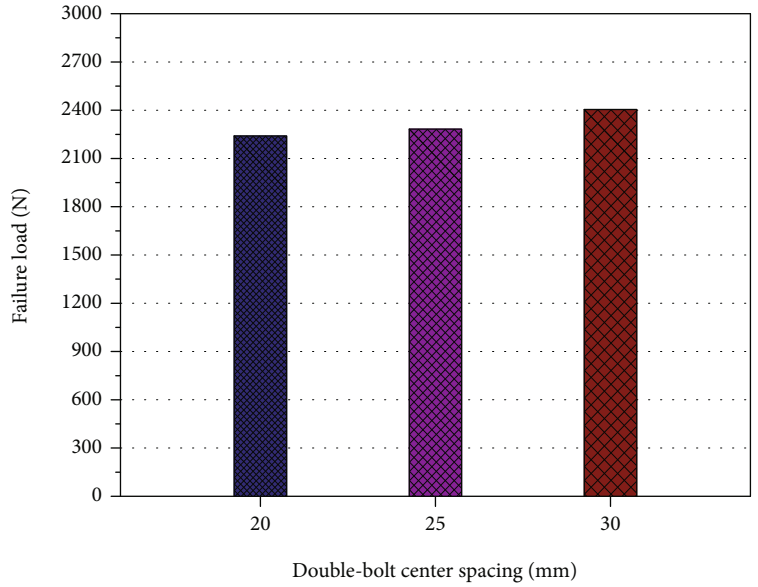

Figure 14: Variation of the failure load with double-bolt center spacing for the studied CMC/superalloy double bolted joint at 750°C.

to the bearing failure at the critical value of $W/D = 4$ where the tension stress exceeds the bearing stress. Our simulation results for the CMC/superalloy hybrid bolted joint at 750°C did not show obvious improvement in the ultimate failure loads with regard to plate width of the composite joints as reported by the above researchers [27, 28, 30, 31]. However, with the same failure load, larger plate margin distance leads to increase of the cross-sectional area of the specimen, and thus, the strength enhances for the studied joints. All failure elements occur around the inner hole edge of ceramic matrix composite plate. At the plate margin distance of 15 mm-25 mm, there occur matrix compression failure, fiber compression failure, and fiber-matrix shear failure of ceramic matrix composite. When the plate margin distance reaches 30 mm, hole edges of ceramic matrix composite plate exhibit a variety of failure modes: matrix tensile failure, matrix

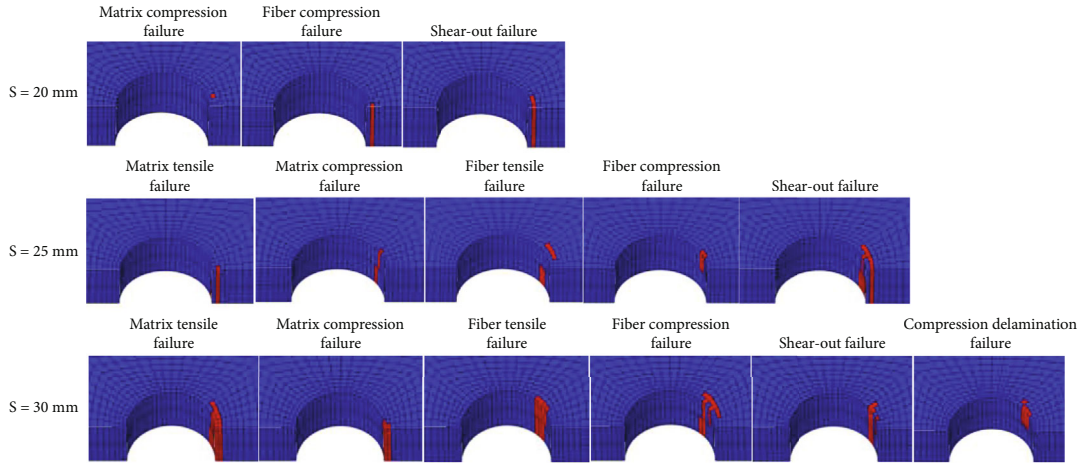

Figure 15: Damage failure patterns around the inner fastener hole of ceramic matrix plate of the double bolted joints with various values of double-bolt center spacing at 750°C.

compression failure, fiber tensile failure, fiber compression failure, and fiber-matrix shear failure at temperature of 750°C.

4.4. Effect of the Double-Bolt Center Spacing of Joints. In order to elucidate the effect of double-bolt center spacing of the mechanical fastened structure on high temperature tensile properties, the load-displacement curves of the joints under uniaxial static tensile loading conditions at 750°C was simulated, and the predicted load-displacements and summarized failure load with double-bolt center spacing for the studied CMC/superalloy double bolted joint at 750°C are shown in Figures 13 and 14, respectively. Compression failure was taken place around hole edge of ceramic-base composite with 35 mm double-bolt spacing at 440°C, and therefore, its load-displacement curve is absent from the Figure 13. It is interesting to note that, in contrast to the load-displacement curve of the 20 mm spacing joint, there is no horizontal section in the curve of joint with 30 mm double-bolt spacing. The possible reason could be that higher double-bolt center spacing brings about the load-carrying level of two bolts more consistent, weakening the successive bearing effect. It can also be observed from the figures that the initial stiffness of the studied connection structure is almost unchanged, whereas the failure load increases slightly from 2240.0 N to 2404.5 N as the double-bolt center spacing increases from 20 mm to 30 mm. Karakuzu et al. [27, 28] also found that the failure load increases with increasing M/D of the woven-glass–vinylester composite plates with two serial pins. However, this parameter is not as effective as the ratio E/D in increasing of failure load. Especially, for $E/D = 1$ specimens, the failure load nearly does not increase with increasing ratio M/D. Tang et al. [31] studied the effects of pitch (p) for 3D C–Cs DBS joint on failure loading and on the failure plane stresses. They found that the failure loading increases first and then decreases with the rise of pitch p. When the value of p/D is lower than the critical ratio, the joint strength will increase with the increase of p/D because the interaction behavior among stress fields around the bolts becomes small. When the value of p/D is higher than the critical ratio, the joint strength will decrease with the increase of p/D. The p/D ratio has only a small effect on the failure plane stresses for the DBS joint. The above geometry effect on the tensile properties was not significant for the studied joint at 750°C. Damage failure patterns around the inner hole of ceramic matrix plate with various values of double-bolt center spacing are shown in Figure 15. For the 20-mm double-bolt spacing joint, there occur matrix compression failure and mainly fiber compression failure and fiber-matrix shear failure of composite hole edge. When the double-bolt spacing of the joint reaches 30 mm, matrix tensile failure, matrix compression failure, fiber tensile failure, fiber compression failure, fiber-matrix compression failure, and compression delamination failure are taken place at 750°C. The interactions of six failure modes resulted in maximum failure load of the CMC/superalloy double bolted connection structure at 750°C.

5. Conclusions

In the present work, a 3D finite element model coupled with progressive damage analysis was established to predict uniaxial static tensile behavior of single-lap, double-bolt CMC/superalloy hybrid joint by ABAQUS software at elevated temperature. Influences of geometrical parameters of double bolted joint structures on failure load at 750°C and associated damage mechanisms were studied by using the developed progressive damage analysis method. The results showed that the initial stiffness of the hybrid bolted joints drops with the rise of applied temperature. However, the load-bearing capacity and the associated failure modes of the double-bolt hybrid joints vary significantly with the applied environment temperature, due to changes of assembly parameters caused by large thermal expansion coefficient difference between the ceramic matrix composite material and the superalloy material at the application of environment temperature. Larger edge distance will change the stress concentration around hole edge of ceramic matrix composite plate as well as the bolt tightening efficiency,

leading to increase first and then decrease in the high temperature load-bearing capacity of the double bolted joint structure. As not effective as the edge distance, the plate margin distance and double-bolt center spacing have little impact on the failure load of the connection structure at 750°C, but the strength of the studied joint improves as the plate margin distance rises. There is no horizontal section in the curve of joint with 30 mm double-bolt spacing, possibly because higher double-bolt center spacing brings about more consistent load-carrying level of two bolts, weakening the successive bearing effect. The ceramic matrix composite failure for the hybrid connection structures changes significantly with respect to different geometric configurations, which mainly occurs in the right side of the inner hole edge of ceramic matrix composite plate. The interactions of multiple failure modes resulted in variations of failure load of the CMC/superalloy double bolted connection structure at elevated temperatures. The present work provides useful information on geometric design and high temperature load-bearing efficiency optimization of ceramic matrix composite connection structure in the development of reusable space transportation systems.

Data Availability

The data used to support the findings of this study are available from the corresponding author upon request.

Conflicts of Interest

The authors declare that there is no conflict of interest regarding the publication of this paper.

Acknowledgments

This work was supported by the Pre-Research Foundation of Shenyang Aircraft Design and Research Institute, Aviation Industry Corporation of China (Grant No. JH20128255), supported by the National Defence Basic Research Program (Grant No. JZ20180032), and supported by the Pre-Research Foundation of Equipment Development Department of People's Republic of China Central Military Commission (Grant No. ZJJSN20200001).

References

[1] R. Naslain, "Design, preparation and properties of non-oxide CMCs for application in engines and nuclear reactors: an overview," *Computer Science and Technology*, vol. 64, no. 2, pp. 155–170, 2004.

[2] D. Hansel, H. Hald, and F. Ruhle, *Development of a Joining Method for High Temperature Constructions, ESA SP-428*, ESA, Paris, 1999.

[3] M. Dogigli, K. Handrick, M. Bickel, and A. Frohlich, "CMC key technologies -background, status," in *Present and Future Applications. ESA SP-521*, ESA, Paris, 2003.

[4] H. Bohrk and U. Beyermann, "Secure tightening of a CMC fastener for the heat shield of re-entry vehicles," *Composite Structures*, vol. 92, no. 1, pp. 107–112, 2010.

[5] K. Wei, Y. Peng, K. Wang, F. Yang, S. Cheng, and T. Zeng, "High temperature mechanical properties of lightweight C/SiC composite pyramidal lattice core sandwich panel," *Composite Structures*, vol. 178, pp. 467–475, 2017.

[6] K. Wei, X. M. Cheng, F. H. Mo, W. B. Wen, and D. N. Fang, "Design and analysis of integrated thermal protection system based on lightweight C/SiC pyramidal lattice core sandwich panel," *Materials and Design*, vol. 111, pp. 435–444, 2016.

[7] X. W. Wang, K. Wei, Y. Tao et al., "Thermal protection system integrating graded insulation materials and multilayer ceramic matrix composite cellular sandwich panels," *Composite Structures*, vol. 209, pp. 523–534, 2019.

[8] D. Glass, "Ceramic matrix composite (CMC) thermal protection systems (TPS) and hot structures for hypersonic vehicles," in *15th AIAA international space planes and hypersonic systems and technologies conference*, p. 2682, Dayton, Ohio, 2008.

[9] H. Weihs, "The SHEFEXII Thermal Protection System," in *Symposium on Aerothermodynamics for Space Vehicles. DLR*, Belgien, 2011.

[10] D. E. Glass, "European directions for hypersonic thermal protection systems and hot structures," in *The 31st Annual Conference on Composites Materials and Structures*, Daytona Beach, FL, 2007.

[11] B. G. Kiral, "Effect of the clearance and interference-fit on failure of the pin-loaded composites," *Materials & Design*, vol. 31, no. 1, pp. 85–93, 2010.

[12] C. T. McCarthy and M. A. McCarthy, "Three-dimensional finite element analysis of single-bolt, single-lap composite bolted joints: part II—effects of bolt-hole clearance," *Composite Structures*, vol. 71, no. 2, pp. 159–175, 2005.

[13] M. A. McCarthy, C. T. McCarthy, V. P. Lawlor, and W. F. Stanley, "Three-dimensional finite element analysis of single-bolt, single-lap composite bolted joints: part I—model development and validation," *Composite Structures*, vol. 71, no. 2, pp. 140–158, 2005.

[14] M. A. McCarthy, V. P. Lawlor, W. F. Stanley, and C. T. McCarthy, "Bolt-hole clearance effects and strength criteria in single-bolt, single-lap, composite bolted joints," *Composites Science and Technology*, vol. 62, no. 10-11, pp. 1415–1431, 2002.

[15] C. T. McCarthy, M. A. McCarthy, and V. P. Lawlor, "Progressive damage analysis of multi-bolt composite joints with variable bolt- hole clearances," *Composites: Part B*, vol. 36, no. 4, pp. 290–305, 2005.

[16] B. Egan, C. T. McCarthy, M. A. McCarthy, and R. M. Frizzell, "Stress analysis of single-bolt, single-lap, countersunk composite joints with variable bolt-hole clearance," *Composite Structures*, vol. 94, no. 3, pp. 1038–1051, 2012.

[17] T. L. Qin, L. B. Zhao, and J. Y. Zhang, "Fastener effects on mechanical behaviors of double-lap composite joints," *Composite Structures*, vol. 100, pp. 413–423, 2013.

[18] A. Olmedo, C. Santiuste, and E. Barbero, "An analytical model for the secondary bending prediction in single-lap composite bolted-joints," *Composite Structures*, vol. 111, pp. 354–361, 2014.

[19] M. Chishti, C. H. Wang, R. S. Thomson, and A. C. Orifici, "Numerical analysis of damage progression and strength of countersunk composite joints," *Composite Structures*, vol. 94, no. 2, pp. 643–653, 2012.

[20] M. Chishti, C. H. Wang, R. S. Thomson, and A. C. Orifici, "Experimental investigation of damage progression and

strength of countersunk composite joints," *Composite Structures*, vol. 94, no. 3, pp. 865–873, 2012.

[21] L. Q. Liu, J. Q. Zhang, K. K. Chen, and H. Wang, "Combined and interactive effects of interference fit and preloads on composite joints," *Chinese Journal of Aeronautics*, vol. 27, no. 3, pp. 716–729, 2014.

[22] C. P. Yang, G. Q. Jiao, B. Wang, T. Huang, and H. B. Guo, "Damage-based failure theory and its application to 2D-C/SiC composites," *Composites: Part A*, vol. 77, pp. 181–187, 2015.

[23] H. Mei, L. F. Cheng, Q. Q. Ke, and L. T. Zhang, "High-temperature tensile properties and oxidation behavior of carbon fiber reinforced silicon carbide bolts in a simulated re-entry environment," *Carbon*, vol. 48, no. 11, pp. 3007–3013, 2010.

[24] G. D. Li, X. F. Wu, C. R. Zhang, H. F. Hu, Y. D. Zhang, and Z. B. Zhang, "Theoretical simulation and experimental verification of C/SiC joints with pins or bolts," *Materials and Design*, vol. 53, pp. 1071–1076, 2014.

[25] L. B. Zhao, W. Yang, T. C. Cao et al., "A progressive failure analysis of all-C/SiC composite multi-bolt joints," *Composite Structures*, vol. 202, pp. 1059–1068, 2018.

[26] B. Okutan and R. Karakuzu, "The strength of pinned joints in laminated composites," *Composites Science and Technology*, vol. 63, no. 6, pp. 893–905, 2003.

[27] R. Karakuzu, N. Taylak, B. Muratten, and M. Akta, "Effects of geometric parameters on failure behavior in laminated composite plates with two parallel pin-loaded holes," *Composite Structures*, vol. 85, no. 1, pp. 1–9, 2008.

[28] R. Karakuzu, R. C. Cihan, M. Akta, and B. M. Icten, "Failure behavior of laminated composite plates with two serial pin-loaded holes," *Composite Structures*, vol. 82, no. 2, pp. 225–234, 2008.

[29] N. A. Kishore, S. K. Malhotra, and P. N. Siva, "Failure analysis of multi-pin joints in glass fibre/epoxy composite laminates," *Composite Structures*, vol. 91, no. 3, pp. 266–277, 2009.

[30] M. Ozen and O. Sayman, "Failure loads of mechanical fastened pinned and bolted composite joints with two serial holes," *Composites Part B Engineering*, vol. 42, no. 2, pp. 264–274, 2011.

[31] Y. L. Tang, Z. G. Zhou, S. D. Pan, J. Xiong, and Y. Guo, "Mechanical property and failure mechanism of 3D Carbon-Carbon braided composites bolted joints under unidirectional tensile loading," *Materials & Design*, vol. 65, no. 65, pp. 243–253, 2015.

[32] G. D. Li, Y. D. Zhang, C. R. Zhang, H. F. Hu, S. Chen, and Z. B. Zhang, "Design, preparation and properties of online-joints of C/SiC-C/SiC with pins," *Composites Part B Engineering*, vol. 48, pp. 134–139, 2013.

[33] C. Lv, S. Y. Zhao, Z. Y. Li et al., "Bolt design of ceramic matrix composite and superalloy bolted joint based on damage failure load," *Journal of Harbin Institute of Technology (New Series)*, vol. 28, no. 2, pp. 55–61, 2021.

[34] S. Y. Zhao, J. L. Dong, C. Lv, Z. Y. Li, X. Y. Sun, and W. J. Zhang, "Thermal mismatch effect and high-temperature tensile performance simulation of hybrid CMC and superalloy bolted joint by progressive damage analysis," *International Journal of Aerospace Engineering*, vol. 2020, Article ID 8739638, 14 pages, 2020.

[35] Z. Junhua, *Design Guides for Missile and Rocket Composite Material Structure, [M.S. thesis]*, China Astronautic Publishing House, Beijing CHN, 1999.

[36] F. Sidoroff, *Description of anisotropic damage application to elasticity*, Berlin-verlag: Springer, 1981.

[37] S. Baste, "Inelastic behaviour of ceramic-matrix composites," *Composites Science and Technology*, vol. 61, no. 15, pp. 2285–2297, 2001.

[38] J. Li, *Research on the Nonlinear Constitutive Relationship of 2D C/SiC Composites*, Northwestern Polytechnical University, 2014.

[39] G. Camus, "Modelling of the mechanical behavior and damage processes of fibrous ceramic matrix composites: application to a 2-D SiC/SiC," *International Journal of Solids and Structures*, vol. 37, no. 6, pp. 919–942, 2000.

[40] O. Siron and P. J. Lamon, "Modelling of the stress/strain behaviour of a carbon/carbon composite with a 2.5 dimensional fibre architecture under tensile and shear loads at room temperature," *Composites Science and Technology*, vol. 59, no. 1, pp. 1–12, 1999.

[41] S. W. Tsai and E. M. Wu, "A general theory of strength for anisotropic materials," *Journal of Composite Materials*, vol. 5, no. 1, pp. 58–80, 1971.

[42] A. D. Sisu, H. H. Hussein, and S. M. Sargand, "The use of Hashin damage criteria, CFRP–concrete Interface and concrete damage plasticity models in 3D finite element modeling of retrofitted reinforced concrete beams with CFRP sheets," *Arabian Journal for Science & Engineering*, vol. 42, no. 3, pp. 1171–1184, 2017.

[43] A. Olmedo and C. Santiuste, "On the prediction of bolted single-lap composite joints," *Composite Structures*, vol. 94, no. 6, pp. 2110–2117, 2012.

[44] S. C. Tan, "A progressive failure model for composite laminates containing openings," *Journal of Composite Materials*, vol. 25, no. 5, pp. 556–577, 1991.

[45] C. Lv, F. Li, S. Y. Zhao, Q. Sun, M. R. Li, and X. Y. Sun, "Influence of assembly parameters on tensile behavior of hybrid CMC and superalloy bolted joints by progressive damage analysis," *Journal of Harbin Institute of Technology (New Series)*, vol. 28, no. 3, pp. 53–60, 2021.